NANO LETTERS

Subscriber access provided by YORK UNIV

Communication

2-Level Quantum Systems in 2-D Materials for Single Photon Emission

Sunny Gupta, Ji-Hui Yang, and Boris I. Yakobson

Nano Lett., **Just Accepted Manuscript** • DOI: 10.1021/acs.nanolett.8b04159 • Publication Date (Web): 11 Dec 2018

Downloaded from http://pubs.acs.org on December 12, 2018

Just Accepted

"Just Accepted" manuscripts have been peer-reviewed and accepted for publication. They are posted online prior to technical editing, formatting for publication and author proofing. The American Chemical Society provides "Just Accepted" as a service to the research community to expedite the dissemination of scientific material as soon as possible after acceptance. "Just Accepted" manuscripts appear in full in PDF format accompanied by an HTML abstract. "Just Accepted" manuscripts have been fully peer reviewed, but should not be considered the official version of record. They are citable by the Digital Object Identifier (DOI®). "Just Accepted" is an optional service offered to authors. Therefore, the "Just Accepted" Web site may not include all articles that will be published in the journal. After a manuscript is technically edited and formatted, it will be removed from the "Just Accepted" Web site and published as an ASAP article. Note that technical editing may introduce minor changes to the manuscript text and/or graphics which could affect content, and all legal disclaimers and ethical guidelines that apply to the journal pertain. ACS cannot be held responsible for errors or consequences arising from the use of information contained in these "Just Accepted" manuscripts.

ACS Publications

is published by the American Chemical Society. 1155 Sixteenth Street N.W., Washington, DC 20036

Published by American Chemical Society. Copyright © American Chemical Society. However, no copyright claim is made to original U.S. Government works, or works produced by employees of any Commonwealth realm Crown government in the course of their duties.

2-Level Quantum Systems in 2-D Materials for Single Photon Emission

Sunny Gupta, Ji-Hui Yang, and Boris I. Yakobson*

Department of Materials Science and Nanoengineering, Department of Chemistry, and the Smalley Institute, Rice University, Houston, Texas 77005, USA

Abstract

Single photon emission (SPE) by a solid state source requires presence of a distinct two-level quantum system, usually provided by point defects. Here we note that a number of qualities offered by novel, two dimensional materials—their all-surface openness and optical transparence, tighter quantum confinement, and reduced charge screening—are advantageous for achieving an ideal SPE. Based on first principles calculations and point-group symmetry analysis, a strategy is proposed to design paramagnetic defect complex with reduced symmetry, meeting all the requirements for SPE: its electronic states are well isolated from the host material bands, belong to a majority spin eigenstate, and can be controllably excited by polarized light. The defect complex is thermodynamically stable, and appears feasible for experimental realization, to serve as a SPE-source, essential for quantum computing, with $Re_{Mo}V_S$ in MoS_2 as one most practical candidate.

Keywords: Photonic qubits, color centers, paramagnetic defects, transition metal dichalcogenides, diamane, boron nitride, ab initio.

Creating photonic qubits for quantum information processing needs materials platform-source capable of single-photon emission (SPE).[1–4] Ideal SPE requires a two-level quantum system with a ground state and an excited state, which can be initialized (brought into definite spin state, perhaps by external magnetic field) and perturbed by an external stimulus (light) to emit a single photon at a time.[5] For minimal decoherence,[6] these states must be well insulated from the bulk or external environment. In a solid-state realization this requires the defect levels to be isolated in energy from the band edges of the host semiconductor and be localized in real space, i.e. have a smaller Bohr radius (a_d). The two-level system must ideally be fully polarized in both absorption and emission channels and have short excited state lifetime (or high radiative rate (k_r)).[5] With this in mind, the paramagnetic defects in a solid-state material forming localized bound states can act as two-level system for SPE. Another requirement which is paramount for an ideal SPE is that the two levels of the paramagnetic defect must preferably belong to a spin doublet configuration. As an electronic excitation in a spin triplet configuration usually involves one or more nonradiative transitions between states of different spin multiplicity and is not preferred for SPE. In the past, a number of solid-state systems, such as trapped single molecules,[7] quantum dots,[8,9] and color centers (NV) in diamond[10,11] have shown SPE. However, these sources emit in the visible range and not in the optimal for optical fiber telecommunication range of 1.2-1.5 μm (~0.77-1 eV). Furthermore, the high refractive index of the host material for SPE often limits the photon-extraction efficiency from these sources.

On the other hand, so called two-dimensional (2D) semiconductors are only few atoms thin and have the natural advantages for SPE. First, an obvious structural "openness"[12] and light-transparency[13] of 2D eliminate the issues of photon extraction. Second, on a less obvious level, due to quantum confinement effect and reduced screening 2D materials tend to have defect states more isolated from the band edges, as desired.[14–16] Third, the effective defect Bohr radius ($a_d \propto \varepsilon$, ε being the dielectric constant) is also much smaller due to reduced screening in 2D. Forth, the radiative rate (k_r) and the oscillator strength (f_{osc}) of the optical transition between defect electronic levels will likely be higher in 2D due to reduced screening and smaller a_d ($k_r \propto f_{osc} \propto 1/a_d^3$).[17,18] It was also shown that the Franck Condon (FC) shift associated with defects in 2D transition-metal dichalcogenides (TMD) is small,[19] which enhances radiative efficiency of the transitions. Interestingly, these attributes of defects in 2D semiconductors are detrimental for doping, when it is required for (opto-) electronic devices;[20] however, it makes them better candidates as the host systems for SPE.

Among 2D materials, TMD have attracted significant attention due to their semiconducting electronic structure exhibiting appealing electronic[21–24] and optical properties.[13,23,25–28] And recently, 2D TMD have even found an application as host materials for single-photon emission (SPE), essential for creating photonic qubits for quantum information processing.[3] In fact, stable SPE has already been observed in 2D TMD[29–32] and hexagonal boron nitride *h*-BN.[33–38] In these works, the SPE in TMD was associated with excitons bound to impurities, and in *h*-BN it was ascribed to crystallographic defects. However, the exact nature of defect states responsible for SPE in these materials remains unclear. With a band gap varying within ~0.5 - 4.5 eV,[39] TMD include a wide range of materials, which makes a general strategy to create a two-level system meeting the above criteria highly sought for or even necessary.

Based on first-principles calculations, we herein propose a strategy to identify and design defects which can form an efficient two-level system in TMD and other 2D materials. The approach is based on perturbing the relation between the defect's atomic configuration (point group symmetry) and its electronic structure. Our study will help understanding and design of practical two-level defect systems in 2D materials, essential for SPE, creating photonic qubits for quantum information processing.

We begin by comparing a N_CV_C defect (N substituted C site next to a C-vacancy) commonly known as NV center, in diamond and its 2D counterparts (Fig. 1a-c). Formally, the thinnest ultimate diamond slab[40] would be graphane[41]—a fully hydrogenated graphene CH (Figure 1a), where each C is sp^3-hybridized and the band gap is ~3.5 eV; however, it is too thin to host a proper NV defect: removing a C entails a loss of adjacent H, and within the gap such defect yields only one singlet state (Fig. 1d), useless for SPE (details of methodology in SI-1, Supporting Information). Next thinnest film of diamond would be a bilayer diamane (Fig. 1b),[42,43] with the exterior carbon bonds passivated with H, as in graphane. The NV defect levels are shown in Figure 1e, along with the diamond case in Figure 1f. The NV defect in both diamond and diamane is paramagnetic and forms a two-level system, with the levels away from band edges. The band gap 3.2 eV in diamane is less than 4.2 eV in diamond (despite the expected trend due to quantum confinement in 2D). The reduced screening in diamane does shrink the defect's effective Bohr radius (~5.5 Å, less than 7 Å in diamond) and accelerates radiative electronic transition rate up to 1 GHz for the 2.02 eV transition in diamane (Figure 1e), versus 97 MHz—order of magnitude less—for the 1.42 eV transition in diamond (Figure 1f); see SI-2 for details of calculations. With the defect levels located far from band edges in both

diamond and diamane, the lower Bohr radius and higher radiative rate in the latter, makes diamane superior to diamond[5] as a host system for SPE.

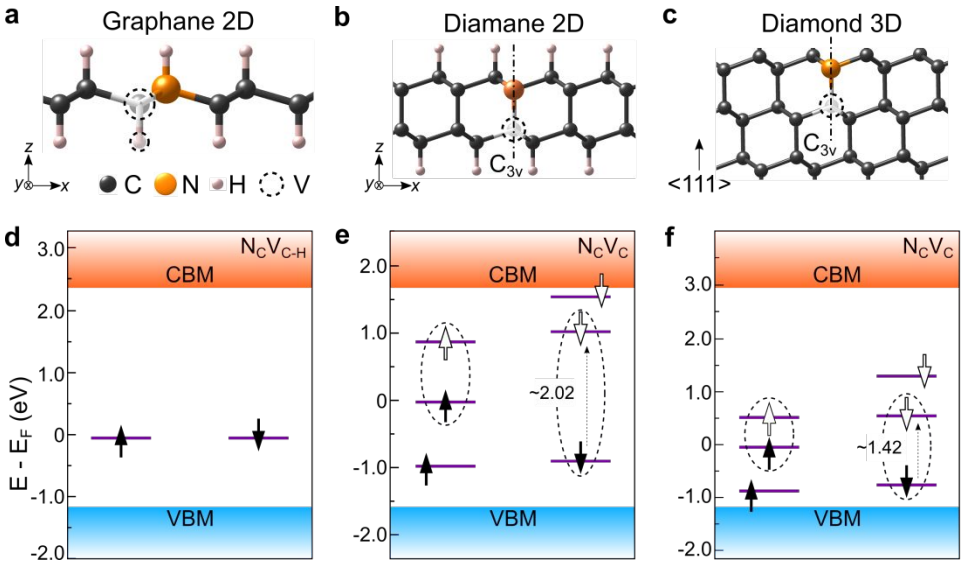

Figure 1. Crystal structure of (a) graphane, (b) diamane, and (c) diamond, with NV defect. Defect levels for neutral NV defect in (d) graphane, (e) diamane, and (f) diamond, calculated using PBE functional. The majority and minority spin states of defects are shown by up ↑ and down ↓ arrows. The states above Fermi level are unoccupied and are shown by unfilled arrows. The two-level systems in both materials are marked with dashed ellipses.

Although diamane is thermodynamically stable in theory,[43] and even detected in experiments,[44,45] it remains far from readily available (however, see [46]). Therefore, we next assess the defects in more common 2D materials, notably a most stable 2*H* phase of monolayer MoS_2—an archetypal TMD. It can host different point defects in forms of atom-vacancies, substitutions, antisites, adatoms, and interstitials. Out of all the possible defects in 2D MoS_2, sulfur vacancy (V_S) and Re substitution of Mo (Re_{Mo}) were found to have the lowest formation energy.[47] V_S is the most commonly observed defect in 2D MoS_2.[47–49] Since as-grown MoS_2 is predominantly found to be *n*-type, recent theoretical study[47] suggests V_S to be most stable in -1 charge state. Re_{Mo} defect has also been observed experimentally[50,51] and is most stable in its neutral charge state.[47] We first discuss the electronic structure of these defects and assess their possible role in SPE.

To avoid defect-image interactions, we simulate defects in a 6x6 supercell (108 atoms), corresponding to a low concentration ~$1.5 \cdot 10^{13}$/cm^2. V_S or Re_{Mo} were created by removing or replacing the corresponding atoms (Figure 2a,c). For sulfur vacancy, its most stable, negatively charged state V_S^- was modeled by adding an extra electron to the system, compensated by positive background.

For the Re_{Mo} defect in Figure 2c, its energy levels are found to lie inside the band gap of MoS_2, as marked purple in Figure 2d. The corresponding charge density is localized at the Re site, Figure 2c. Re_{Mo} in its neutral charge state is paramagnetic, with a magnetic moment of 1 μ_B. The unpaired electron arises from an extra valence of Re substituting Mo. The occupied defect level at ~0.1 eV below the conduction band minimum (CBM) is a shallow defect state. This defect

level is not well isolated from the band edges and (unlike V_S^-, discussed next) the Re_{Mo} defect levels do not form a feasible two-level system. (Notably, shallow defect states like of Re_{Mo} could be readily ionized and used to *n*-dope the MoS_2.)

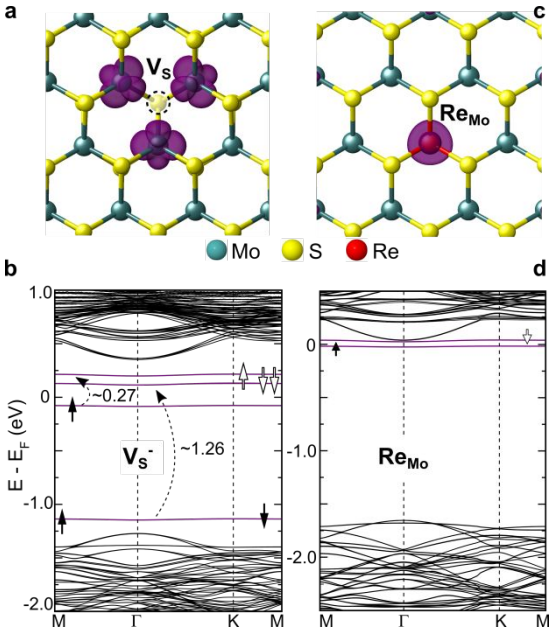

Figure 2. Optimized geometries of the defects in the MoS_2 layer: (a) V_S and (c) Re_{Mo}. The iso-charge density corresponding to HOMO is shown in purple. The calculated band structure of supercell with (b) V_s^- and (d) neutral Re_{Mo} defect, using PBE functional with SOC. The defect levels shown in purple are dispersionless. The majority and minority spin states of defects are shown by up ↑ and down ↓ arrows. The states above Fermi level are unoccupied, as marked by unfilled arrows. Possible electronic transitions are shown by dashed arrows.

For the V_S defect, its charge density has a C_{3v} symmetry (same as NV defect in diamond, Figure 1c) and is localized on the nearest Mo atoms surrounding the S vacancy, Figure 2a. The band structure computed using PBE functional with spin-orbit coupling (SOC) for the supercell (Figure 2b) preserves the band gap ~1.63 eV of pristine MoS_2; it appears at Γ point instead of *K* point, due to band folding by the enlarged supercell. All defect levels associated with V_S^- are shown in purple and lie inside the MoS_2 band gap. While the lowest occupied defect level at ~0.13 eV above the valence band maximum (VBM) is spin-degenerate, the HOMO level is non-degenerate with one unpaired electron due to the negative charge of V_S^-, making it paramagnetic with a moment 1 μ_B. Note that, the HOMO level in V_S^- will recover its degeneracy if V_S^- turns to neutral V_S after removing the additional electron (Figure S2 in SI). With the negative charge, the degenerate levels are found to split due to a combined effect of SOC and Jahn-Teller (JT) distortion associated with the defect, and thus they form a two-level system with an energy difference of ~0.27 eV. Apart from this the defect levels in V_S^- form another two-level system between the lowest occupied and highest unoccupied eigenstates of minority (↓) spin. These states energies are separated by ~1.26 eV and the corresponding excitation is shown in Figure 2b. The electronic excitations associated with both of these two-level systems were found to have non-zero electric transition dipole matrix elements, meaning that they are allowed by

symmetry and can be excited by light. Hence, both two-level systems of V_S^- defect seem in principle to serve for SPE.

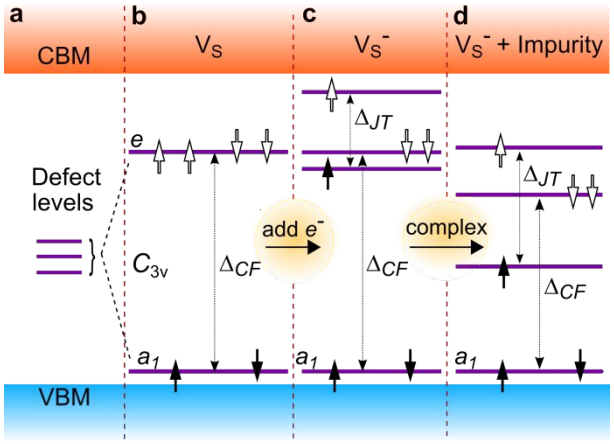

Figure 3. Schematic describing the design strategy to create an ideal two-level system from point defects. (a) Defect bands in a point defect (vacancy) splits according to its symmetry. (b) V_S has C_{3v} symmetry and its defect states splits into a_1 (occupied) and e (empty) levels due to the crystal field (CF) of the host. The defect is non-paramagnetic, therefore (c) an addition of an extra e^- in V_S i.e. charged defect, further splits the e levels due to JT distortion and creates a two-level system. The energy levels are not isolated from band edges making then not ideal for SPE. (d) Addition of a paramagnetic impurity such as making a defect complex adds an extra e^- to the neutral V_S and perturbs both CF and JT energies creating an ideal two-level system. Thus, adding a paramagnetic impurity next to a vacancy defect will be favorable to create an ideal two-level system.

However, these two-state quantum systems do not meet the criterion described earlier for SPE: the V_S^- levels are not sufficiently isolated from the host band edges. The highest unoccupied defect level is only ~150 meV below the conduction band (Figure 2b). This value is comparable to the linewidth of ~100-150 meV due to electron-phonon coupling associated with CBM in TMD[52,53] at room temperature. Therefore, the two-level quantum state in V_S^- defect can only function for SPE at low T.

To have the defect operational at room temperature, its levels must be shifted towards the middle of the band gap. To this end, we first retrace the relation between defect's atomic configuration (point group symmetry) and its electronic structure. V_S defect has a C_{3v} symmetry with lower occupied a_1 level and higher unoccupied e level (Figure 3b) (a_1 and e are the symmetry elements of C_{3v} symmetry); the splitting between a_1 and e levels is due to the crystal field (CF) of the host. Further, the presence of an extra electron in V_S^- creates a paramagnetic state and also splits the majority spin level of e by a combined effect of JT distortion and SOC. This splitting shifts the unoccupied level closer to CBM, in undesirable proximity to continuum (Figure 2b and 3c). To remedy this situation and move the e levels towards the middle of the band gap, Δ_{CF} and Δ_{JT} must be altered. These energy splits depend on the host environment surrounding the defect. Therefore, adding an impurity next to the defect can help by perturbing Δ_{CF} and Δ_{JT} values, Figure 3d. We find, through direct computations, that adding a Re substitution at Mo site (Re has one extra e^-, lies to the right of Mo in the periodic table and makes a paramagnetic impurity) near the S vacancy $Re_{Mo}+V_S = Re_{Mo}V_S$ (Figure 4a), indeed significantly alters the defect levels. Re adds an extra electron and perturbs Δ_{JT}, while the presence of this additional defect of course also

alters Δ_{CF}. We show below that the electronic levels in this defect complex are significantly improved and are optimal for SPE. This design strategy of adding a paramagnetic impurity next to a vacancy defect appears efficient in creating the two-level systems for SPE. We find later that this approach is general for any point defect with C_{3v} or D_{3h} symmetry in TMD and other 2D materials, as further examples demonstrate.

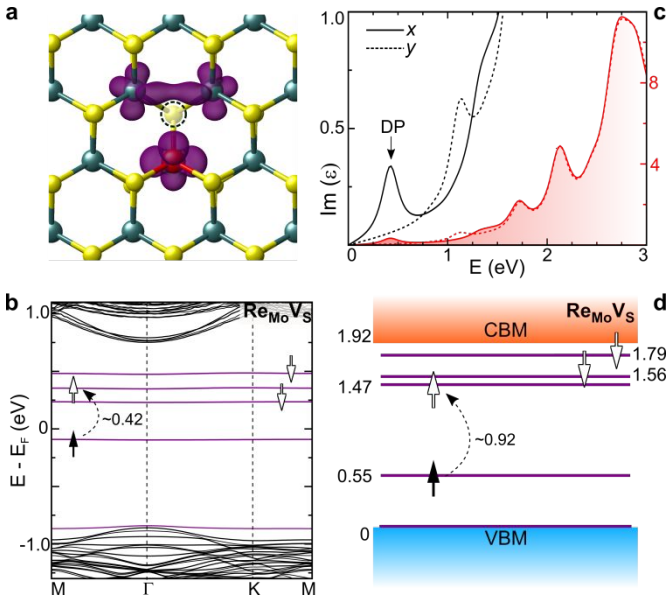

Figure 4. (a) Optimized geometry of $Re_{Mo}V_S$ defect in the 2D MoS_2 layer. The iso-charge density surface of the defect HOMO, shown in purple, is localized on nearby atoms. (b) The band structure of supercell with $Re_{Mo}V_S$ defect calculated using PBE functional with SOC. The defect levels are shown in purple. The majority and minority spin states of defect are marked by up and down arrows. A dashed arrow shows possible electronic ~0.42 eV transition. The states above Fermi level are unoccupied and are shown by unfilled arrows. (c) The imaginary part of the dielectric function Im $\varepsilon(\omega)$; the spectra for *x* and *y* polarization directions are shown by solid and dashed lines, respectively, and display a defect peak (DP) at ~0.42 eV. The scales on the left and right are different and correspond to the same plot. (d) The electronic levels of defect computed using HSE functional with SOC.

We first use PBE functional with SOC to find that the electronic levels of neutral $Re_{Mo}V_S$ defect lie inside the band gap of MoS_2 (Figure 4b, purple dispersionless horizontals). The charge density corresponding to the highest occupied state is localized on nearby atoms (Figure 4a, also purple). The defect in its neutral charge state has an unpaired electron and is paramagnetic with doublet spin configuration. The minority-spin states of the defect are unoccupied, while the majority spin-states form a two-level system with highest occupied ground state and empty excited state. These defect levels are well isolated from the host band edges and are separated in energy by ~0.42 eV due to perturbed Δ_{CF} and Δ_{JT}. This two-level state can be excited with a laser pulse, provided the electronic transition is allowed by symmetry. To examine this, we calculated the dipole matrix elements for all possible electronic transitions in MoS_2 with $Re_{Mo}V_S$ defect, and then evaluated the imaginary part of the dielectric function Im $\varepsilon(\omega)$, directly related with the absorbance spectra of the material. Calculated under random phase approximation, Im $\varepsilon(\omega)$ along *x* and *y* polarization directions is shown in Figure 4c. The peaks there at $E > 1.6$ eV correspond to interband transitions in the host material MoS_2. The optical transitions associated with defect levels can be seen in the lower energy region. The electronic excitation associated with the two-

level defect state has a non-zero electric transition dipole matrix element only for *x*-polarized light (Figure 4c). A clear peak at ~0.42 eV corresponding to this defect transition can be seen in Figure 4c. This polarization-selective excitation provides an additional control of the defects emission, advantageous for SPE. The peak at ~1.2 eV in Figure 4c corresponds to an excitation from the VBM to the minority spin-state and can be seen only for *y*-polarized light. We also find that creating a defect complex with a non-paramagnetic impurity such as $W_{Mo}V_S$ instead of $Re_{Mo}V_S$ does not form a two-level system. Thus a paramagnetic impurity is an important consitutent of the defect chemistry required to create a two level system.

The electronic structure with PBE (GGA) functional suffers from underestimating the band gap as it does not correctly account for the self-interactions and derivative discontinuity in the exchange-correlation energy.[54] Moreover, for an accurate description of the electronic structure and optical spectra, excitonic effects must be considered with *GW*+BSE formalism. The latter is computationally very demanding for a large system considered here. We find for MoS_2 (as also known for numerous examples) that due to self-cancellation of errors the estimates of electronic eigenstates with hybrid HSE[55] functional matches very well with experiments. The value of band gap ~1.92 eV calculated with HSE functional (Figure 4d) compares very well with the A-exciton peak (optical gap) seen in the experimental optical spectra of MoS_2 at ~1.9 eV.[56,57] Therefore, the defect levels should also be accurately estimated with HSE functional, and the results of both HSE (~0.92 eV) and PBE (~0.42 eV) functionals are shown in Figure 4b,d. The transition energy is still much smaller than the optical gap ~1.9 eV of MoS_2 and thus $Re_{Mo}V_S$ defect remains good for SPE. In experiments the emitters are initially not at zero-strain because of various imperfections during sample fabrication such as wrinkles, cracks, and lattice mismatches, that would perturb the electronic levels of the defect.[38] We evaluated the effect of strain on the electronic levels of $Re_{Mo}V_S$ defect in MoS_2 (see SI-11, in SI). The optical transition associated with the two-levels in $Re_{Mo}V_S$ shows a dependence of 14.5 meV/% and -24.37 meV/% with strain along the armchair and zigzag direction, respectively (notably few times weaker than the strain modulation of the host-material bandgap). On the other hand, this can be advantageous for strain tuning of quantum emission.[38]

Another technologically important parameter of two-level system is the count rate of emission, equal to radiative rate k_r times the probability $k_r/(k_r+k_n)$ of radiation transition, with k_n being the rate of non-radiative relaxation. We calculated the radiative rate ($1/\tau_r$, an inverse of radiative lifetime) of the optical transition associated with the two-level system in $Re_{Mo}V_S$. For the transiton ΔE = 0.92 eV in Figure 4d a value of k_r = 5 GHz or τ_r = 0.2 ns was obtained. This lifetime for $Re_{Mo}V_S$ defect is two orders of magnitude shorter than τ_r = 10 - 30 ns[5,58] observed for NV center in diamond, thereby signifying the advantage of defects in 2D over 3D systems. Since this defect is an odd electron system with just one electron (S = 1/2), the spin-states with different spin multiplicity (S = 0,1,3/2) are not allowed. The defect cannot exist in any other spin-state and the only non-radiative transition from excited state is back to the ground state. We estimate the rate for this non-radiative process (see SI-12, in SI) and obtain k_n = 0.1 MHz, which is four orders of magnitude smaller than radiative rate, signifying the quantum efficiency to be >99.99%.

Since most of the 2D materials synthesized till now have a coordination number of 3 or 6, a vacancy in these systems will either have C_{3v} or D_{3h} symmetry. The defect structure proposed

above, to create an SPE two-level system by adding a paramagnetic impurity next to a vacancy of C_{3v} or D_{3h} symmetry, suggests a general strategy. To test it, we apply this design to other 2D materials such as WS_2, WSe_2, ZrS_2 and boron nitride (*h*-BN). All the constructed defect complexes indeed exhibit two-level systems, with the transition energies shown in Table 1 (see Figure S3 in SI for the electronic levels of the defects), and thus affirm the validity of our approach. This way of defect chemistry modification can be used to create a two-level system in a variety of 2D materials for SPE. We would also like to point out that the NV defects in diamane or diamond (Figure 1b,c) discussed above also suits such design scheme, and in fact was an initial motivation. There, point defect V_C has a C_{3v} symmetry while N substitution (due to its extra electron relative to C) acts as a paramagnetic impurity. Notably, out of all the defects considered here, only $Re_{Mo}V_S$ offers a transition in the optical fiber telecommunication band (Table 1). The calculated zero-phonon line (ZPL) emission (accounting for the structural relaxation) of $Re_{Mo}V_S$ defect is at 0.77 eV (Figure S10, in SI), which is very close to the commonly used erbium transition around ~0.8 eV (1.53 - 1.6 μm, depending on Er concentration) in fiber telecommunications. All the above designed defects are paramagnetic (like NV centers) and can in principle be also used for spin qubits. The spin states can be initialized by applying an external magnetic field and be read out by an optical excitation. This direct spin-based utility is however beyond the scope of present study, focused on SPE.

Table 1: Constituents of defect complex in different host 2D systems. The paramagnetic impurity has an extra e^- and lies to the right of the substituent atom in the periodic table. The vacancy has a C_{3v} or D_{3h} symmetry. The transition energy of the two-level system formed by the defect complex, band gap of host material, and the distance of two-level system from CBM and VBM is calculated using HSE functional. The ZPL emission value for $Re_{Mo}V_S$ defect is also shown.

Host	Vacancy (Point group symmetry)	Paramagnetic Impurity	Defect Complex	Transition Energy (ZPL) (eV)	Band Gap (eV)	From CBM/VBM (eV)
MoS_2	**V_S (C_{3v})**	**Re_{Mo}**	**$Re_{Mo}V_S$**	**0.92 (0.77)**	**1.92**	**0.45/0.55**
WSe_2	V_{Se} (C_{3v})	Re_W	Re_WV_{Se}	1.09	1.82	0.25/0.48
ZrS_2	V_S (C_{3v})	Ta_{Zr}	$Ta_{Zr}V_S$	0.32	1.74	0.32/1.1
BN	V_N (D_{3h})	C_B	C_BV_N	1.74	5.25	0.76/2.75
WS_2	V_S (C_{3v})	Re_W	Re_WV_S	1.17	2.08	0.35/0.56
Diamane	V_C (C_{3v})	N_C	N_CV_C	3.06	3.95	0.32/0.57
Diamond	V_C (C_{3v})	N_C	N_CV_C	2.49	5.25	2.41/0.35

One should also discuss the thermodynamic stability and the feasibility of creating this ($Re_{Mo}V_S$) defect in experiments. To this end, our computations (see SI-5, in SI) show that indeed the formation of $Re_{Mo}V_s$ complex from preexisting (as observed in experiments[47–51]) Re_{Mo} and V_s is thermodynamically favorable; it can likely form by diffusion of mobile vacancies towards substitutional Re. Furthermore, we find that this defects is preferred in its neutral charge state (see SI-5, in SI), which is paramagnetic as required, for a reasonably broad range of the Fermi level (Figure S4, in SI; outside of this identified range the positive or negative states are

nonmagnetic and therefore are suboptimal for SPE). Another possible way of engineering this desirable defect ex-situ can be through e-beam irradiation of a MoS_2 sample doped with Re, and quantitative analysis (Figure S8, in SI) shows that the displacement threshold for S knockout is much lower in the proximity of Re_{Mo}, favoring the formation of exactly desirable defect-complex.

In summary, presented first-principles calculations have quantified and highlighted the advantages of 2D materials as host systems for SPE. For various 2D materials—diamane (C), MoS_2, WS_2, WSe_2, ZrS_2, and *h*-BN—the analysis predicts specific defects, whose electronic levels form ideal two-level quantum systems essential for SPE. Then a general scheme is proposed for creating a defect complex by adding a paramagnetic impurity adjacent to a vacancy defect, to obtain a proper two-level system. This scheme can be extended to other 2D materials with C_{3v} or D_{3h} symmetry which includes a number of TMD and oxides. Out of all possible defects considered, we find electronic transitions in $Re_{Mo}V_S$ defect in MoS_2 to lie in the optimal range for optical telecommunication. The occupied defect levels in neutral $Re_{Mo}V_S$ have a spin doublet configuration and can be selectively excited with light polarized along zigzag direction *x*, thereby providing an additional control to exploit its functionality. $Re_{Mo}V_S$ defect complex has a positive binding energy (relative to the individual Re_{Mo} and V_S) and can likely be created in-situ in a real material. A two-step procedure is also proposed for ex-situ creation of $Re_{Mo}V_S$ defect in experiment using electron beam irradiation. Our theoretical analysis uncovers the tantalizing electronic properties of 2D materials as host systems for SPE and also predicts optimal two-level quantum systems, which can be used as a source for single photons required in quantum information processing.

ASSOCIATED CONTENT

Supporting Information

This material is available free of charge via the Internet at http://pubs.acs.org/. The Supporting Information is available free of charge on the ACS Publications website at DOI:

Methodology, Bohr radius and radiative rate calculation, electronic levels of V_S defect in neutral charge state, electronic levels of designed defect complex in other 2D materials, details about thermodynamic stability, in-situ creation and defect formation energy calculations and correction of charge-state-transition level, electronic levels of $Re_{Mo}V_S$ defect in +1, and -1 charge state, details for formation energy of $Re_{Mo}V_S$ defect in different growth conditions, ex-situ creation of defect with e-beam irradiation and atom displacement cross section using the McKinley-Feshbach formalism, effect of strain, non-radiative rate and convergence test.

AUTHOR INFORMATION

Corresponding Author

*Email: biy@rice.edu

Notes

The authors declare no competing financial interest.

ACKNOWLEDGMENTS

The authors acknowledge the DAVinCI-Center for Research Computing at Rice University, DoD HPCMP, and National Energy Research Scientific Computing Center (NERSC), a U.S. Department of Energy Office of Science User Facility for computational resources. SG would like to thank Sharmila N. Shirodkar and Alex Kutana for helpful discussions. This work was supported by the Army Research Office grant W911NF-16-1-0255, and in part (graphane, diamane and qubits motivation) by the Office of Naval Research grant N00014-15-1-2372.

References

(1) Kok, P.; Munro, W. J.; Nemoto, K.; Ralph, T. C.; Dowling, J. P.; Milburn, G. J. Linear Optical Quantum Computing with Photonic Qubits. *Rev. Mod. Phys.* **2007**, *79*, 135–174. https://doi.org/10.1103/RevModPhys.79.135.

(2) O'Brien, J. L.; Furusawa, A.; Vučković, J. Photonic Quantum Technologies. *Nat. Photonics* **2009**, *3*, 687–695. https://doi.org/10.1038/nphoton.2009.229.

(3) Aharonovich, I.; Englund, D.; Toth, M. Solid-State Single-Photon Emitters. *Nat. Photonics* **2016**, *10*, 631–641. https://doi.org/10.1038/nphoton.2016.186.

(4) He, X.; Htoon, H.; Doorn, S. K.; Pernice, W. H. P.; Pyatkov, F.; Krupke, R.; Jeantet, A.; Chassagneux, Y.; Voisin, C. Carbon Nanotubes as Emerging Quantum-Light Sources. *Nat. Mater.* **2018**, *17*, 663–670. https://doi.org/10.1038/s41563-018-0109-2.

(5) Aharonovich, I.; Castelletto, S.; Simpson, D. A.; Su, C.-H.; Greentree, A. D.; Prawer, S. Diamond-Based Single-Photon Emitters. *Rep. Prog. Phys.* **2011**, *74*, 076501. https://doi.org/10.1088/0034-4885/74/7/076501.

(6) Chirolli, L.; Burkard, G. Decoherence in Solid-State Qubits. *Adv. Phys.* **2008**, *57*, 225–285. https://doi.org/10.1080/00018730802218067.

(7) Basché, T.; Moerner, W. E.; Orrit, M.; Talon, H. Photon Antibunching in the Fluorescence of a Single Dye Molecule Trapped in a Solid. *Phys. Rev. Lett.* **1992**, *69*, 1516–1519. https://doi.org/10.1103/PhysRevLett.69.1516.

(8) Michler, P.; Imamoğlu, A.; Mason, M. D.; Carson, P. J.; Strouse, G. F.; Buratto, S. K. Quantum Correlation among Photons from a Single Quantum Dot at Room Temperature. *Nature* **2000**, *406*, 968–970. https://doi.org/10.1038/35023100.

(9) Michler, P.; Kiraz, A.; Becher, C.; Schoenfeld, W. V.; Petroff, P. M.; Zhang, L.; Hu, E.; Imamoglu, A. A Quantum Dot Single-Photon Turnstile Device. *Science* **2000**, *290*, 2282–2285. https://doi.org/10.1126/science.290.5500.2282.

(10) Gruber, A.; Dräbenstedt, A.; Tietz, C.; Fleury, L.; Wrachtrup, J.; Borczyskowski, C. von. Scanning Confocal Optical Microscopy and Magnetic Resonance on Single Defect Centers. *Science* **1997**, *276*, 2012–2014. https://doi.org/10.1126/science.276.5321.2012.

(11) Kurtsiefer, C.; Mayer, S.; Zarda, P.; Weinfurter, H. Stable Solid-State Source of Single Photons. *Phys. Rev. Lett.* **2000**, *85*, 290–293. https://doi.org/10.1103/PhysRevLett.85.290.

(12) Zou, X.; Yakobson, B. I. An Open Canvas—2D Materials with Defects, Disorder, and Functionality. *Acc. Chem. Res.* **2015**, *48*, 73–80. https://doi.org/10.1021/ar500302q.

(13) Gupta, S.; Shirodkar, S. N.; Kutana, A.; Yakobson, B. I. In Pursuit of 2D Materials for Maximum Optical Response. *ACS Nano* **2018**, *12*, 10880–10889. https://doi.org/10.1021/acsnano.8b03754.

(14) Noh, J.-Y.; Kim, H.; Park, M.; Kim, Y.-S. Deep-to-Shallow Level Transition of Re and Nb Dopants in Monolayer MoS2 with Dielectric Environments. *Phys. Rev. B* **2015**, *92*, 115431. https://doi.org/10.1103/PhysRevB.92.115431.

(15) Singh, A.; Manjanath, A.; Singh, A. K. Engineering Defect Transition-Levels through van Der Waals Heterostructure. *J. Phys. Chem. C* **2018**, *122*, 24475–24480. https://doi.org/10.1021/acs.jpcc.8b08082.

(16) Wang, D.; Han, D.; Li, X.-B.; Xie, S.-Y.; Chen, N.-K.; Tian, W. Q.; West, D.; Sun, H.-B.; Zhang, S. B. Determination of Formation and Ionization Energies of Charged Defects in Two-Dimensional Materials. *Phys. Rev. Lett.* **2015**, *114*, 196801. https://doi.org/10.1103/PhysRevLett.114.196801.

(17) Takagahara, T. Biexciton States in Semiconductor Quantum Dots and Their Nonlinear Optical Properties. *Phys. Rev. B* **1989**, *39*, 10206–10231. https://doi.org/10.1103/PhysRevB.39.10206.

(18) Shimura, T.; Matsuura, M. Binding Energy and Oscillator Strength of Excitonic Molecules in Type-II Quantum Wells. *Phys. Rev. B* **1997**, *56*, 2109–2113. https://doi.org/10.1103/PhysRevB.56.2109.

(19) Gupta, S.; Shirodkar, S. N.; Kaplan, D.; Swaminathan, V.; Yakobson, B. I. Franck Condon Shift Assessment in 2D MoS 2. *J. Phys. Condens. Matter* **2018**, *30*, 095501. https://doi.org/10.1088/1361-648X/aaa93e.

(20) Yang, J.-H.; Yakobson, B. I. Dimensionality-Suppressed Chemical Doping in 2D Semiconductors: The Cases of Phosphorene, MoS2, and ReS2 from First-Principles. *ArXiv171105094 Cond-Mat* **2017**.

(21) Lembke, D.; Bertolazzi, S.; Kis, A. Single-Layer MoS2 Electronics. *Acc. Chem. Res.* **2015**, *48*, 100–110. https://doi.org/10.1021/ar500274q.

(22) Jariwala, D.; Sangwan, V. K.; Lauhon, L. J.; Marks, T. J.; Hersam, M. C. Emerging Device Applications for Semiconducting Two-Dimensional Transition Metal Dichalcogenides. *ACS Nano* **2014**, *8*, 1102–1120. https://doi.org/10.1021/nn500064s.

(23) Kis, A.; Coleman, J. N.; Kalantar-Zadeh, K.; Strano, M. S.; Wang, Q. H. Electronics and Optoelectronics of Two-Dimensional Transition Metal Dichalcogenides. *Nat. Nanotechnol.* **2012**, *7*, nnano.2012.193. https://doi.org/10.1038/nnano.2012.193.

(24) Radisavljevic, B.; Radenovic, A.; Brivio, J.; Giacometti, V.; Kis, A. Single-Layer MoS2 Transistors. *Nat. Nanotechnol.* **2011**, *6*, 147–150. https://doi.org/10.1038/nnano.2010.279.

(25) Eda, G.; Yamaguchi, H.; Voiry, D.; Fujita, T.; Chen, M.; Chhowalla, M. Photoluminescence from Chemically Exfoliated MoS2. *Nano Lett.* **2011**, *11*, 5111–5116. https://doi.org/10.1021/nl201874w.

(26) Lopez-Sanchez, O.; Lembke, D.; Kayci, M.; Radenovic, A.; Kis, A. Ultrasensitive Photodetectors Based on Monolayer MoS2. *Nat. Nanotechnol.* **2013**, *8*, 497–501. https://doi.org/10.1038/nnano.2013.100.

(27) Yin, Z.; Li, H.; Li, H.; Jiang, L.; Shi, Y.; Sun, Y.; Lu, G.; Zhang, Q.; Chen, X.; Zhang, H. Single-Layer MoS2 Phototransistors. *ACS Nano* **2012**, *6*, 74–80. https://doi.org/10.1021/nn2024557.

(28) Chernikov, A.; Berkelbach, T. C.; Hill, H. M.; Rigosi, A.; Li, Y.; Aslan, O. B.; Reichman, D. R.; Hybertsen, M. S.; Heinz, T. F. Exciton Binding Energy and Nonhydrogenic Rydberg Series in Monolayer WS2. *Phys. Rev. Lett.* **2014**, *113*, 076802. https://doi.org/10.1103/PhysRevLett.113.076802.

(29) Srivastava, A.; Sidler, M.; Allain, A. V.; Lembke, D. S.; Kis, A.; Imamoğlu, A. Optically Active Quantum Dots in Monolayer WSe_2. *Nat. Nanotechnol.* **2015**, *10*, 491–496. https://doi.org/10.1038/nnano.2015.60.

(30) He, Y.-M.; Clark, G.; Schaibley, J. R.; He, Y.; Chen, M.-C.; Wei, Y.-J.; Ding, X.; Zhang, Q.; Yao, W.; Xu, X.; Lu, C. Y.; Pan, J.W. Single Quantum Emitters in Monolayer Semiconductors. *Nat. Nanotechnol.* **2015**, *10*, 497–502. https://doi.org/10.1038/nnano.2015.75.

(31) Koperski, M.; Nogajewski, K.; Arora, A.; Cherkez, V.; Mallet, P.; Veuillen, J.-Y.; Marcus, J.; Kossacki, P.; Potemski, M. Single Photon Emitters in Exfoliated WSe_2 Structures. *Nat. Nanotechnol.* **2015**, *10*, 503–506. https://doi.org/10.1038/nnano.2015.67.

(32) Tonndorf, P.; Schmidt, R.; Schneider, R.; Kern, J.; Buscema, M.; Steele, G. A.; Castellanos-Gomez, A.; Zant, H. S. J. van der; Vasconcellos, S. M. de; Bratschitsch, R. Single-Photon Emission from Localized Excitons in an Atomically Thin Semiconductor. *Optica* **2015**, *2*, 347–352. https://doi.org/10.1364/OPTICA.2.000347.

(33) Bourrellier, R.; Meuret, S.; Tararan, A.; Stéphan, O.; Kociak, M.; Tizei, L. H. G.; Zobelli, A. Bright UV Single Photon Emission at Point Defects in H-BN. *Nano Lett.* **2016**, *16*, 4317–4321. https://doi.org/10.1021/acs.nanolett.6b01368.

(34) Martínez, L. J.; Pelini, T.; Waselowski, V.; Maze, J. R.; Gil, B.; Cassabois, G.; Jacques, V. Efficient Single Photon Emission from a High-Purity Hexagonal Boron Nitride Crystal. *Phys. Rev. B* **2016**, *94*, 121405. https://doi.org/10.1103/PhysRevB.94.121405.

(35) Tran, T. T.; Bray, K.; Ford, M. J.; Toth, M.; Aharonovich, I. Quantum Emission from Hexagonal Boron Nitride Monolayers. *Nat. Nanotechnol.* **2016**, *11*, 37–41. https://doi.org/10.1038/nnano.2015.242.

(36) Tran, T. T.; Elbadawi, C.; Totonjian, D.; Lobo, C. J.; Grosso, G.; Moon, H.; Englund, D. R.; Ford, M. J.; Aharonovich, I.; Toth, M. Robust Multicolor Single Photon Emission from Point Defects in Hexagonal Boron Nitride. *ACS Nano* **2016**, *10*, 7331–7338. https://doi.org/10.1021/acsnano.6b03602.

(37) Chejanovsky, N.; Rezai, M.; Paolucci, F.; Kim, Y.; Rendler, T.; Rouabeh, W.; Fávaro de Oliveira, F.; Herlinger, P.; Denisenko, A.; Yang, S.; Gerhardt, I.; Finkler, A.; Smet, J. H.;,Wrachtrup. J. Structural Attributes and Photodynamics of Visible Spectrum Quantum Emitters in Hexagonal Boron Nitride. *Nano Lett.* **2016**, *16*, 7037–7045. https://doi.org/10.1021/acs.nanolett.6b03268.

(38) Grosso, G.; Moon, H.; Lienhard, B.; Ali, S.; Efetov, D. K.; Furchi, M. M.; Jarillo-Herrero, P.; Ford, M. J.; Aharonovich, I.; Englund, D. Tunable and High-Purity Room Temperature Single-Photon Emission from Atomic Defects in Hexagonal Boron Nitride. *Nat. Commun.* **2017**, *8*, 705. https://doi.org/10.1038/s41467-017-00810-2.

(39) Rasmussen, F. A.; Thygesen, K. S. Computational 2D Materials Database: Electronic Structure of Transition-Metal Dichalcogenides and Oxides. *J. Phys. Chem. C* **2015**, *119*, 13169–13183. https://doi.org/10.1021/acs.jpcc.5b02950.

(40) Muñoz, E.; Singh, A. K.; Ribas, M. A.; Penev, E. S.; Yakobson, B. I. The Ultimate Diamond Slab: GraphAne versus GraphEne. *Diam. Relat. Mater.* **2010**, *19*, 368–373. https://doi.org/10.1016/j.diamond.2010.01.007.

(41) Sofo, J. O.; Chaudhari, A. S.; Barber, G. D. Graphane: A Two-Dimensional Hydrocarbon. *Phys. Rev. B* **2007**, *75*, 153401. https://doi.org/10.1103/PhysRevB.75.153401.

(42) Chernozatonskii, L. A.; Sorokin, P. B.; Kvashnin, A. G.; Kvashnin, D. G. Diamond-like C2H Nanolayer, Diamane: Simulation of the Structure and Properties. *JETP Lett.* **2009**, *90*, 134–138. https://doi.org/10.1134/S0021364009140112.

(43) Kvashnin, A. G.; Chernozatonskii, L. A.; Yakobson, B. I.; Sorokin, P. B. Phase Diagram of Quasi-Two-Dimensional Carbon, From Graphene to Diamond. *Nano Lett.* **2014**, *14*, 676–681. https://doi.org/10.1021/nl403938g.

(44) Martins, L. G. P.; Matos, M. J. S.; Paschoal, A. R.; Freire, P. T. C.; Andrade, N. F.; Aguiar, A. L.; Kong, J.; Neves, B. R. A.; Oliveira, A. B. de; Mazzoni, M. S. C.; Filho, A. G. S; Cançado, L. G. Raman Evidence for Pressure-Induced Formation of Diamondene. *Nat. Commun.* **2017**, *8*, 96. https://doi.org/10.1038/s41467-017-00149-8.

(45) Gao, Y.; Cao, T.; Cellini, F.; Berger, C.; Heer, W. A. de; Tosatti, E.; Riedo, E.; Bongiorno, A. Ultrahard Carbon Film from Epitaxial Two-Layer Graphene. *Nat. Nanotechnol.* **2018**, *13*, 133–138. https://doi.org/10.1038/s41565-017-0023-9.

(46) Diamane. http://terramonstersworldgalaxy.wikia.com/wiki/Diamane.

(47) Komsa, H.-P.; Krasheninnikov, A. V. Native Defects in Bulk and Monolayer MoS2 from First Principles. *Phys. Rev. B* **2015**, *91*, 125304. https://doi.org/10.1103/PhysRevB.91.125304.

(48) Fabbri, F.; Rotunno, E.; Cinquanta, E.; Campi, D.; Bonnini, E.; Kaplan, D.; Lazzarini, L.; Bernasconi, M.; Ferrari, C.; Longo, M.; Nicotra, G.; Molle, A.; Swaminathan, V.; Salviati, G. Novel Near-Infrared Emission from Crystal Defects in MoS2 Multilayer Flakes. *Nat. Commun.* **2016**, *7*. https://doi.org/10.1038/ncomms13044.

(49) Qiu, H.; Xu, T.; Wang, Z.; Ren, W.; Nan, H.; Ni, Z.; Chen, Q.; Yuan, S.; Miao, F.; Song, F.; Long, G.; Shi, Y.; Sun, L.; Wang, J.; Wang, X. Hopping Transport through Defect-Induced Localized States in Molybdenum Disulphide. *Nat. Commun.* **2013**, *4*, 2642. https://doi.org/10.1038/ncomms3642.

(50) Lin, Y.-C.; Dumcenco, D. O.; Komsa, H.-P.; Niimi, Y.; Krasheninnikov, A. V.; Huang, Y.-S.; Suenaga, K. Properties of Individual Dopant Atoms in Single-Layer MoS2: Atomic Structure, Migration, and Enhanced Reactivity. *Adv. Mater.* **2014**, *26*, 2857–2861. https://doi.org/10.1002/adma.201304985.

(51) Kochat, V.; Apte, A.; Hachtel, J. A.; Kumazoe, H.; Krishnamoorthy, A.; Susarla, S.; Idrobo, J. C.; Shimojo, F.; Vashishta, P.; Kalia, R.; Nakano, A.; Tiwary, C. S.; Ajayan, P. M. Re Doping in 2D Transition Metal Dichalcogenides as a New Route to Tailor Structural Phases and Induced Magnetism. *Adv. Mater.* **2017**, *29*, 1703754. https://doi.org/10.1002/adma.201703754.

(52) Molina-Sánchez, A.; Palummo, M.; Marini, A.; Wirtz, L. Temperature-Dependent Excitonic Effects in the Optical Properties of Single-Layer MoS2. *Phys. Rev. B* **2016**, *93*, 155435. https://doi.org/10.1103/PhysRevB.93.155435.

(53) Hinsche, N. F.; Ngankeu, A. S.; Guilloy, K.; Mahatha, S. K.; Grubišić Čabo, A.; Bianchi, M.; Dendzik, M.; Sanders, C. E.; Miwa, J. A.; Bana, H.; Travaglia, E.; Lacovig, P.; Bignardi, L.; Larciprete, R.; Baraldi, A.; Lizzit, S.; Thygesen, K. S.; Hofmann, P. Spin-Dependent Electron-Phonon Coupling in the Valence Band of Single-Layer WS2. *Phys. Rev. B* **2017**, *96*, 121402. https://doi.org/10.1103/PhysRevB.96.121402.

(54) Perdew, J. P. Density Functional Theory and the Band Gap Problem. *Int. J. Quantum Chem.* **1985**, *28*, 497–523. https://doi.org/10.1002/qua.560280846.

(55) Heyd, J.; Scuseria, G. E.; Ernzerhof, M. Hybrid Functionals Based on a Screened Coulomb Potential. *J. Chem. Phys.* **2003**, *118*, 8207–8215. https://doi.org/10.1063/1.1564060.

(56) Mak, K. F.; Lee, C.; Hone, J.; Shan, J.; Heinz, T. F. Atomically Thin MoS2: A New Direct-Gap Semiconductor. *Phys. Rev. Lett.* **2010**, *105* (13), 136805. https://doi.org/10.1103/PhysRevLett.105.136805.

(57) Okada, M.; Kutana, A.; Kureishi, Y.; Kobayashi, Y.; Saito, Y.; Saito, T.; Watanabe, K.; Taniguchi, T.; Gupta, S.; Miyata, Y.; Yakobson, B. I.; Shinohara, H.; Kitaura, R. Direct and Indirect Interlayer Excitons in a van Der Waals Heterostructure of HBN/WS2/MoS2/HBN. *ACS Nano* **2018**, *12*, 2498–2505. https://doi.org/10.1021/acsnano.7b08253.

(58) Goss, J. P.; Jones, R.; Breuer, S. J.; Briddon, P. R.; Öberg, S. The Twelve-Line 1.682 EV Luminescence Center in Diamond and the Vacancy-Silicon Complex. *Phys. Rev. Lett.* **1996**, *77*, 3041–3044. https://doi.org/10.1103/PhysRevLett.77.3041.

TOC